Materials Science-Poland, 29(2), 2011, pp. 143-151
http://www.materialsscience.pwr.wroc.pl/
DOI: 10.2478/s13536-011-0021-9

VERSITA

$(Bi_2Te_3)_{0.25}(Sb_2Te_3)_{0.75}$ crystal structure improvements with excess Te as studied by AFM, SEM, EBSD and XRD

G. KAVEI*, K. AHMADI, A.-K. SHADMEHR, A. KAVEI,

Material and Energy Research Centre, P.O. Box 14155-4777, Tehran, Iran

$(Bi_2Te_3)_x(Sb_2Te_3)_{1-x}$ solid solutions with $x = 0.2$, 0.25 and 0.3 – p type thermoelectric compounds with an excess of Tellurium dopant up to 4 wt% were crystallized. By increasing the Bi_2Te_3 content in the Bi−Sb−Te system, the hole concentration decreased and in consequence caused an optimum Seebeck coefficient and a decrease in electrical conductivity and thermal conductivity, thus resulting in an increase in the figure of merit at $x = 0.25$. The results showed that optimum thermoelectric properties can be achieved for a mixture of $x = 0.25$ with 3 wt% Te added. Structural characterizations of this compound in the absence and presence of the dopant were carried out by means of X-Ray diffraction measurement, scanning electron microscopy, electron backscattering diffraction and atomic force microscopy. Detailed analyses confirm that the improvements in thermoelectric parameters due to the intrinsic structure and minimum defects during crystallization of the compounds result from the excess of Te.

Keywords: *structure homogeneity, intrinsic structure, Atomic Force Microscopy (AFM), Scanning Electron Microscopy (SEM), Electron Backscatter Diffraction (EBSD)*

1. Introduction

Thermoelectric (TE) effects were a little more than a mere curiosity until 1950s, when Ioffe [1] found that doped semiconductors had a larger TE effect than the other materials. There are three main techniques to achieve bismuth telluride crystal growth: based on Bridgman [2], zone-melting [3], and Czochralski [4] methods. Powder metallurgy techniques such as mechanical alloying [5, 6], hot-extrusion methods [7], and hot-pressing [8, 9] are commonly used for the fabrication of TE elements.

Bismuth telluride and antimony telluride, which have the same rhombohedral structure, form a continuous series of solid solutions [10]. Undoped Bi_2Te_3–Sb_2Te_3 alloys are all of p type, and the hole concentration increases markedly toward the Sb_2Te_3 rich region [11]. There have been several comprehensive reports on the influence of chemical composition on TE properties of p type $(Bi_2Te_3)_x(Sb_2Te_3)_{1-x}$ solid solutions, which showed that the figure of merit could be improved by decreasing the lattice thermal conductivity with enhanced phonon scattering due to the lattice distortion, however, there were many discrepancies in the published works [12–16]. Most of the previous works have only focused on the measurements of the basic transport mechanisms to define TE properties. The optimum stoichiometries were tested for the compounds of $(Bi_2Te_3)_x(Sb_2Te_3)_{1-x}$. It was found that $(Bi_2Te_3)_{0.25}(Sb_2Te_3)_{0.75}$ compound was the best p type material with the optimal TE properties.

However, Smirous and Stourac [17] reported a Z value as high as $3.58\times10^{-3}K^{-1}$ at room temperature for a p type $(Bi_2Te_3)_{0.25}(Sb_2Te_3)_{0.75}$ alloy containing 4 wt% excess of Te and 0.05 wt% Ge. Shortly afterwards, Rosi et al. [18] obtained equally high figure of merit (Z) of $3.53\times10^{-3}K^{-1}$ at room temperature for a p type $(Bi_2Te_3)_{0.25}(Sb_2Te_3)_{0.75}$

*E-mail: g-kavei@merc.ac.ir

alloy that was doped with 1.75 wt% excess of Se. Fan et al. [19] introduced polycrystalline *p* type $(Bi,Sb)_2Te_3$ alloys with excess of Te prepared by mechanical alloying and sintering in an activated plasma environment. The effect of an excessive Te content on the TE properties of $Bi_{0.5}Sb_{1.5}Te_3$ and $Bi_{0.4}Sb_{1.6}Te_3$ alloys was studied. The figure of merit decreased when the amount of excess Te increased up to 8 wt%. This should be attributed to the fact that the chemical composition of matrix phase displayed its variations due to the presence of the excesssive Te content and the free Te phase.

To analyze the doping effect on the structure, it is necessary to review the basic structure of Bi_2Te_3. The Bi_2Te_3-based crystals are made-up of atomic layers in the order of $Te^{(1)}$–Bi–$Te^{(2)}$–Bi–$Te^{(1)}$ along *c* axis [20]. Nevertheless, the $(Bi_2Te_3)_x(Sb_2Te_3)_{1-x}$ crystal consists of isomorphous compounds such as Sb_2Te_3 and Bi_2Te_3. Adding elements as dopants of nearly the same atomic size as the compound atoms to a multi-constituent compound will change the material transport properties, possibly in a constructive way. This allows the compound to acquire desirable properties such as low thermal conductivity, an ability to control free carrier concentration, an isoelectronic substitution of different metal ions and decrease in the number of defects in a crystal structure [21].

In this paper, the fabrication of $(Bi_2Te_3)_x(Sb_2Te_3)_{1-x}$ crystals (with $x = 0.20$, 0.25 and 0.30) with an addition of Te up to 4 wt% for achieving optimum TE properties was studied. The structures of the $(Bi_2Te_3)_{0.25}(Sb_2Te_3)_{0.75}$ were characterized by X-Ray Diffraction (XRD), Scanning Electron Microscopy (SEM), and Electron backscatter diffraction (EBSD). Atomic Force Microscopy (AFM) was employed to check the quality of the grown crystal and solid solution phase in the section perpendicular to the direction of the crystal growth right through the ingot core from the surface to the center. This can be a new sensitive technique for crystal structures characterization by AFM images. TE transport properties such as electrical and thermal conductivities and the Seebeck coefficient were measured. The results showed that the crystal structure is constantly modified due to an excessive addition of Te up to 3 %.

2. Material and methods

P type $(Bi_2Te_3)_x(Sb_2Te_3)_{1-x}$ compounds with $x = 0.2$, 0.25 and 0.3 were fabricated. The experimental details were briefly described in [12]. The optimum chemical composition of $(Bi_2Te_3)_{0.25}(Sb_2Te_3)_{0.75}$ was chosen and extra Te at different fraction of weights up to 4 wt% was added to improve it further. Before the fabrication, Bi, Te and Sb were purified up to 5 N in a vacuum system of 10^{-5} Torr. The degree of purity and the chemical elemental analysis were evaluated by Inductively Coupled Plasma-Mass-Atomic Emission Spectrophotometer (ICP-AES model ARL 3410+). Atomic Absorption Spectroscopy (AAS) analysis revealed that there were some fractions of undesired elements in the samples. The analyses were conducted on several elements (Cu, Fe, Ni, Pb and S) by using Graphite Furnace (932 plus, GBC) detection.

Stoichiometric portion of the powder mixtures for $(Bi_2Te_3)_{0.25}(Sb_2Te_3)_{0.75}$ and extra 0–4 wt% Te were filled into a quartz tube; the tube was evacuated below 10^{-5} Torr, followed by heating to 250 °C in a cylindrical furnace to degas the container. Nitrogen or argon gas was introduced into the vacuum system to remove the reacting atmospheric gases such as hydrogen and oxygen. This process assured that the undesired reactions of the atmospheric gases with other elements would not occur at the time when the sintering was in progress. The evacuated tube was sealed at the pressure of 10^{-4} Torr. The quartz tube was placed in a rocking furnace at 700 °C to achieve well stirred melted solid solution. The solution molten in the tube was well stirred at 80 oscillations per minute parallel to the tube axis for one hour to make a homogeneous melt with no segregation. The tube containing the molten solution was quenched at a 200 °C in an oil tank. It was finally cooled down to the room temperature. The solidified ingot was pulverized and filled into a quartz tube of 300 mm length and 8 mm diameter. The tube was evacuated again to 10^{-4} Torr and sealed, then placed in a vertical melting-zone system and was allowed to crystallize the compound at a rate of 13 $mm \cdot h^{-1}$. To improve the homogeneity and quality, the crystallized ingot content was annealed

in the tube at 300 °C for 24 h, then cooled down to room temperature for 5 h. Finally, the crystallized ingot was removed from the tube for study.

The phase analysis was carried out by XRD using a Phillips (30 kV, 20 mA) diffractometer with CuKα radiation ($\lambda = 1.5405$ Å). Morphologies of the samples were examined by a Cambridge SEM operating at 25 kV.

The detection of unknown micrometer-sized phases using the scanning electron microscope (SEM) was limited due to system measuring range. Crystallographic information about unknown micro structure and morphology of the samples was defined by Electron Backscatter Diffraction (EBSD). This technique can provide the background to identify the unknown crystalline phases while exploiting the excellent imaging capabilities of SEM.

The SEM and EBSD examinations were used to evaluate the constituent phases of the samples with and without extra Te but we did not find any differences. These techniques are not sensitive enough to detect a change in the constituent phases or the existence of subsidiary phases. To overcome this problem Scanning Probe Microscopy (SPM) and XRD were used.

SPM is a method to characterize the surface morphology and nanostructure with high precision [22]. For more brittle TE samples, the force interaction between the SPM tip and the sample surface must be minimized to obtain non-destructive imaging. This is done in a tapping mode imaging, which allows an examination to be carried out without damages or surface alteration. Tapping, that is oscillating cantilever probe on a soft or brittle surface, prevents the surface from being damaged by eliminating the lateral forces that exist inherently in a contact mode (where the tip is simply dragged over the surface). To record the AFM images, the cylindrical ingot was cut in half lengthwise to produce two hemicylinders.

SPM used in this study was a Solver Pro, (NT-MDT Ltd., Moscow, Russia) that operates in a None Contact-Atomic Force Microscopy (NC-AFM) also called Tapping mode. The NC-G01S tips used were compatible with most Scanning Probe Microscopy SPM devices with a nominal force constant of 5.5 N·m^{-1}. To record NC-AFM images, some samples were provided with a crystal material cleaved along the growth direction.

The transport properties of TE element i.e. electrical and thermal conductivities and the Seebeck coefficient were measured to determine the influence of excess Te on the compound efficiency. Electrical conductivity was determined by the bar method using a laboratory made device. The measurements were repeated by four point probe and by Hall effect measurements. To prevent errors resulting from the Peltier and Joule effects, the measurements were made rapidly at time intervals shorter than 1s. The thermal conductivity (κ), was defined on the basis of the absolute value definition for semiconductors by using the method described in [23].

The Seebeck coefficient (α) of the ingot is defined from $\frac{\Delta V}{\Delta T}$, taking into account the correction of the thermocouples error, as suggested by [24]. The ΔV and ΔT measurements were carried out by two thermocouples fixed on the ingot at a defined distance. One end of the ingot was heated with a tiny coil heater, generating a temperature gradient from 2 to 3 °C·cm^{-1}. At this point several measurements at a defined interval were accomplished along the ingot.

3. Results and discussion

Structure formation was sensitive to chemical stoichiometry, so the fractions of the elements in the compounds had to be well defined. Characterization of the products was carried out by XRD, SEM, EBDS and AFM. The preferred orientations of grains in the crystals were studied by these methods. The XRD patterns were recorded for different weight fractions of Te added. However, because of indistinguishable peaks positions of the formed phases of Te, apart from insignificant variations of the peak intensities, significant differences between the XRD patterns with extra Te were not observed. Fig. 1 shows the XRD patterns from midsection of the $(Bi_2Te_3)_{0.25}(Sb_2Te_3)_{0.75}$ with 3 wt% extra Te. Miller indices in Fig. 1 are taken from XRD standard data sheet for Bi_2Te_3, Sb_2Te_3 and $Sb_{0.405}Te_{0.595}$ phases. A combination of EBSD and crystallographic XRD database is becoming a standard and sensitive technique for the identification of unknown and semi-crystalline phases in a com-

Table 1. XRD data for the Bi_2Te_3, Sb_2Te_3, $Sb_{0.405}Te_{0.595}$ and $(Bi_2Te_3)_{0.25}(Sb_2Te_3)_{0.75}$ structures.

Bi_2Te_3						$Sb_{0.405}Te_{0.595}$						Sb_2Te_3						$(Bi_2Te_3)_{0.25}(Sb_2Te_3)_{0.75}$					
I	k	h	d(Å)	2θ	I	I	k	h	d(Å)	2θ	I	I	k	h	d(Å)	2θ	I	I	k	h	d(Å)	2θ	I
10	17.738	5.00	0	0	6	–	–	–	–	–	–	4	17.44	5.080	0	0	6	40	17.6	–	0	0	6
100	27.616	3.23	0	1	5	100	28.036	3.18	0	1	5	100	28.244	3.157	0	1	5	100	28.1	–	0	1	5
70	38.131	2.36	1	0	10	100	38.10	2.36	1	0	10	35	38.285	2.349	1	0	10	50	38.2	–	1	0	10
50	40.831	2.210	1	1	0	38	42.194	2.214	1	1	0	6 25	40.700 42.401	2.215 2.130	0 1	1 1	11 0	28	42	–	1	1	0
30	45.439	1.996	0	0	15	63	44.599	2.03	0	0	15	4	44.599	2.030	0	0	15	65	44.8	–	0	0	15
30	50.032	1.823	2	0	5	63	51.438	1.775	2	0	5	2	50.553	1.804	1	1	9	22	51.6	–	2	0	5
5	54.805	1.675	1	0	16	63	54.058	1.695	0	0	18	2	54.162	1.692	0	0	18	30	54.1	–	0	0	18
20	57.256	1.609	0	2	10	63	58.154	1.585	0	2	10	8	58.436	1.578	0	2	10	18	58	–	0	2	10
30	62.454	1.487	1	1	15	63	63.106	1.472	1	0	19	8	63.202	1.470	1	0	19	20	63	–	1	0	19
40	66.553	1.405	1	2	5	63	66.333	1.408	0	1	20	2	66.333	1.408	0	1	20	20	66.2	–	0	1	20

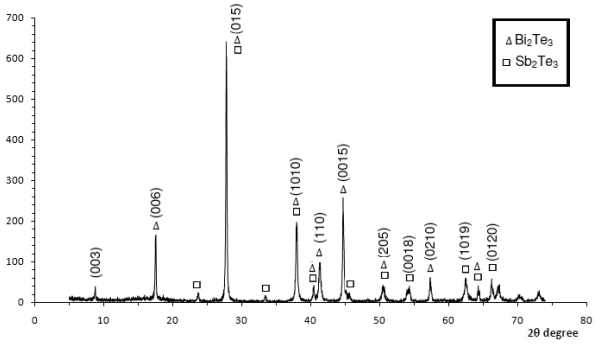

Fig. 1. XRD pattern of powdered $(Bi_2Te_3)_{0.25}$ $(Sb_2Te_3)_{0.75}$ sample with 3 wt% extra Te.

pound. A simple, but impractical approach to phase identification would be to try each set of the data base sequentially to see if the information in the pattern could be simulated. However, it is important to make a distinction between the phase identification and phase verification. The main difference between these two is the number of candidate phases that are to be searched through to find whether they match correctly to the unknown phase. In phase verification, the operator is aware of a phase present in the sample and thus a very small number of choices are to be made (usually less than 5). On the other hand, in a true phase identification process a large database of crystalline compounds is searched through to make any correct recognition with a little input from the operator, [25].

The XRD data sheet in Table 1 shows the intensities of (015), (1010), (110), (0015), (006) and (0210) planes that can be attributed to Bi_2Te_3, Sb_2Te_3. Planes (0018) and (1019) were related to $Sb_{0.405}Te_{0.595}$, which is an unstoichiometric compound of the antimony telluride. It is possible to attribute the unknown crystalline phases by indexing the recorded diffraction patterns from EBSD and use the data from Table 1, [26]. Our data suggests that the extra Te has a significant effect on a) the structure and b) the TE properties of the formed compounds.

3.1. Effect of extra Te on thermoelectric crystal structures

Before adding extra Te into the samples, the TE ingots contained an unintentional phase of

($Sb_{0.405}Te_{0.595}$). The $Sb_{0.405}Te_{0.595}$ phase can behave as a defect in the crystal rather than as a perfect crystal. This is due to the loss of stoichiometry in Te required for the constitution of a chemically stoichiometric compound. The loss arises from low vapor pressure of Te or Te penetration into the tube wall. Adding extra Te into the $Sb_{0.405}Te_{0.595}$ compound eliminated this deficiency but the single phase $(Bi_2Te_3)_{0.25}(Sb_2Te_3)_{0.75}$ was formed at optimum addition only. In practice, phase formation analysis shows no significant difference in the XRD patterns or other analysis from different fraction of Bi_2Te_3 and Sb_2Te_3 since the crystal structures of Bi_2Te_3 and Sb_2Te_3 are the same, (rhombohedral) and the lattice volumes nearly equal. In this case, the theory has not predicted the differences in 2θ, lattice constants and peak intensities between the XRD patterns taken from different fractions of Sb_2Te_3 and the chemically unstoichiometric formed compounds.

SEM was employed to identify the unknown microstructure phases in the compounds. Figs. 2 (a and b) show selected SEM images of a surface of the crystal cleaved along the crystal growth direction (layer structure) in two different scales and systems. The planes of growth are aligned approximately to the growth direction. In addition to XRD and EBDS, numerous images taken by SEM for the samples with different percentage of extra Te, (at different scales and places) did not show any distinguishable differences between the images. To evaluate the constituent phases an attempt was made with EBDS. Figs. 3 (a and b) show the EBSD images that illustrate the constituent phases in $(Bi_2Te_3)_{0.25}(Sb_2Te_3)_{0.75}$ samples without and with 3 wt% extra Te, respectively. There is no detectable difference in the figures either. Nevertheless, the images confirm the perfection of the crystal. It has been concluded that the phase identification with different systems is not too very useful to consider the effect of the excess Te. However, from XRD spectra at large scale it may be possible to evaluate the peaks displacements and intensities interpreting the formed structures divergences.

Figs. 4 (a and b) illustrate representative AFM images of a circular surface (perpendicular to the growth direction) along the radius, 3 mm away from the centre. Figs. 4c–4d were recorded at the center of a hemi-cylinder, which clearly shows a layer structure that correlates with the results obtained by SEM in higher precision. However, the structure observed by AFM reveals the growth process of crystallization in a more regular and perfect fashion. Fig. 4 gives useful information on the microstructure features related to the TE behavior. The figure shows that the growth process was regular and perfect. Analyzing the NC-AFM images in more details requires taking into account the effect of artifacts on the images. This is now one of the unresolved problems which requires a lot of attention to be removed.

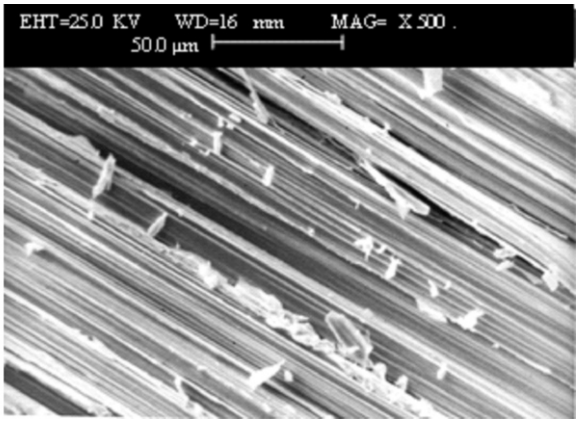

(a)

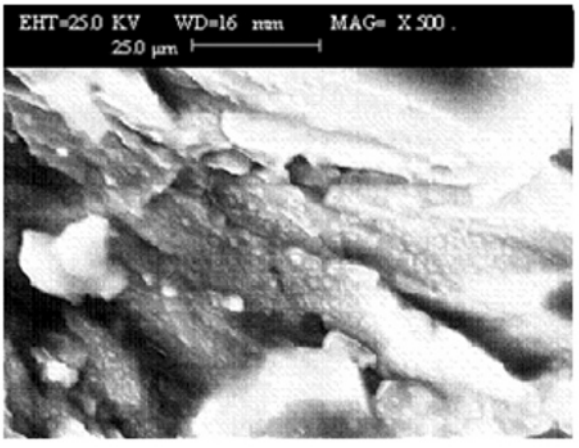

(b)

Fig. 2. SEM images from a cleavage surface of the crystal along the crystal growth direction parallel to *c* axes at: (a) 500 µm; (b) 250 µm scales.

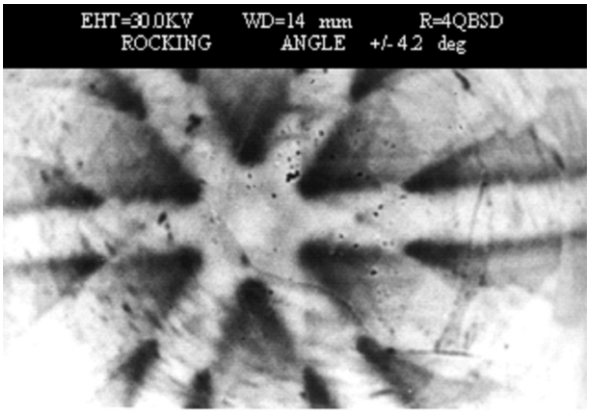

(a)

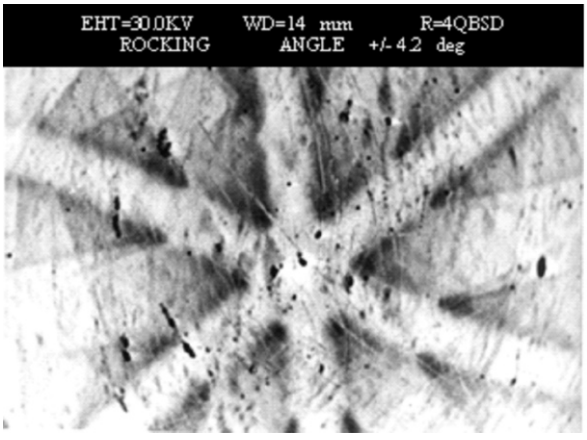

(b)

Fig. 3. EBSD patterns of $(Bi_2Te_3)_{0.25}(Sb_2Te_3)_{0.75}$ samples recorded directly on the film, (a) without extra Te, (b) with 3 wt% extra Te.

3.2. Influence of extra Te on TE properties

Chemical composition has a big influence on the carrier concentration and TE properties. Therefore, the chemical stoichiometry has to be well defined, through the use of analyzing methods such as AAS. It is well known that $(Bi_2Te_3)_x(Sb_2Te_3)_{1-x}$ crystal shows strong anisotropy of TE transport properties. Therefore, the crystal direction for measuring the TE parameters should be considered. Anisotropy variation affects the electrical and thermal conductivities and the Seebeck coefficient along the ingot growth direction [27].

An efficiency of the TE element is expressed by electrical and thermal conductivities and the Seebeck coefficient. Table 2 and Fig. 5 show the Seebeck coefficients, electrical and thermal conductivities and the figures of merit of the crystal ingots with the fraction of added tellurium of 0–4 wt%, to confirm the improvements of the TE properties through the addition of Te. The figure permits an interesting understanding of the obtained data. Excessive Te 0–4 wt% modifies the crystal structure, at optimum of 3 wt% addition. Conclusions can be drawn by evaluating the values of electrical to thermal conductivities (σ/κ) ratios at different percentages and maximum value of the Seebeck coefficient (α) predicted by theory. The Seebeck coefficient, as the most important TE parameter for TE materials in the extrinsic conduction region, is related to the hole concentration for in a p type TE material as follows [28]:

Table 2. Summary data of the Seebeck coefficient, electrical and thermal conductivities of $(Bi_2Te_3)_{0.25}(Sb_2Te_3)_{0.75}$ and the fraction of added tellurium 0–4 wt%, to the ingot.

Parameter/ Added Te	0	1 wt%	2 wt%	3 wt%	4 wt%
$\alpha(\mu V \cdot K^{-1})$	228	230.5	232.5	235	229
$\sigma_H\left((\Omega \cdot cm)^{-1}\right)$	1700	1600	1540	1490	1410
$\kappa\left(W \cdot (mK)^{-1}\right)$	2.9	2.75	2.68	2.6	2.4
$\sigma_H/\kappa(K \cdot V^{-2})$	586.2	581.8	574.6	573.1	587.5
$Z(\times 10^{-3}K^{-1})$	3.07	3.09	3.11	3.17	3.08

$$\alpha = \frac{k_B}{e}\left[S + \frac{5}{2} + \ln\frac{2(2\pi m^* k_B T)^{\frac{3}{2}}}{ph^3}\right] \qquad (1)$$

where k_B is the Boltzmann's constant, S the scattering parameter ($S = 0$ for lattice scattering and 2 for impurity scattering), h is Plank's constant, p the hole density and m^* effective carrier mass. This formula shows that an increment of the Seebeck coefficient can be achieved by decreasing the positive carrier concentration (hole concentration) which results in a reduction of antistructural defects and scattering mechanism of free carriers. This can be achieved by the addition of Te up to 3 wt% At a constant temperature T, the Seebeck coefficient of p type TE materials can be simplified as [29, 30]:

$$\alpha = k_B[S + C + \ln p]/e \qquad (2)$$

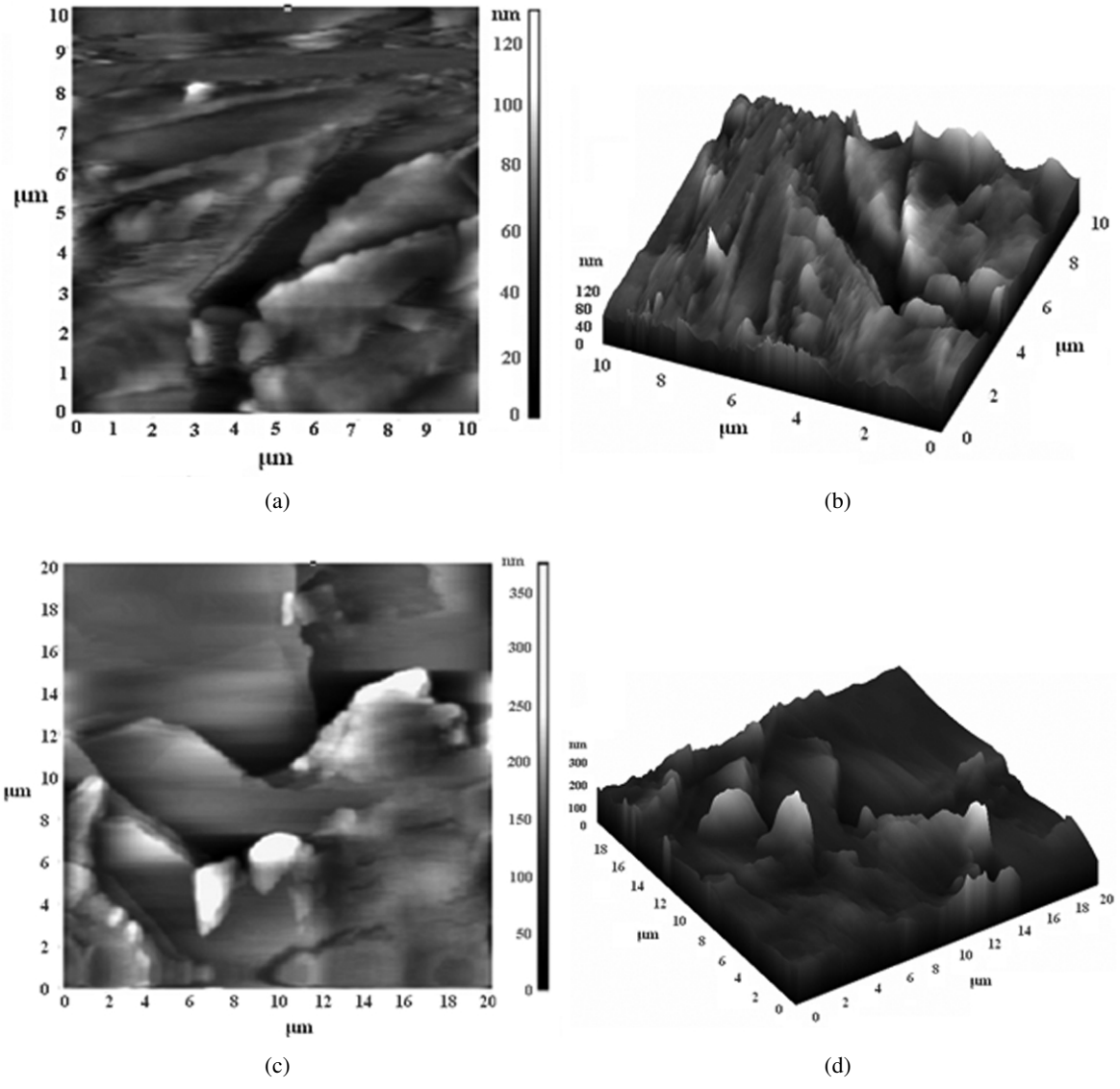

Fig. 4. AFM images in tapping mode from a cleavage surface of the crystal along the crystal growth direction parallel to *c* axes, (a) two-dimensional, (b) three-dimensional with 10 μm scale, 3 mm from the center along the radius of hemi-cylinder (c) two-dimensional and (d) three-dimensional with 20 μm scale, at the center of hemi-cylinder, respectively.

where C is a constant. It can be easily understood that the high Seebeck coefficient of the material arises from the low carrier concentration in the sample.

Generally, TE properties change with temperature in fact with carriers transport in the ingots. On the other hand, the excess Te has a sensitive influence on the variation in the carrier concentration. Therefore, the TE properties at room temperature depend not only on the crystal quality but also (much more) on the carrier concentration. TE measurement only at room temperature cannot give a satisfactory evaluation of the crystal quality.

Based on these measurements, the figure-of-merit (Z) at room temperature was evaluated by:

$$Z = \frac{\alpha^2 \sigma}{\kappa} \tag{3}$$

The Z values of 3.07 to $3.17 \times 10^{-3}\mathrm{K}^{-1}$ at different percentage of Te added were obtained. The

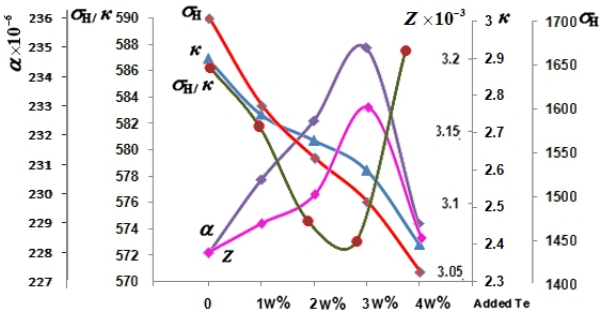

Fig. 5. Variations of α, σ_H, κ, σ_H/κ, and Z are illustrated for comprehensive study of the extra Te effect on the TE transport parameters.

difference between these two values is about 3 %, which seems to be within the range of accuracy of the measurement devices. However, statistical errors of the current measurement techniques for both electrical and thermal conductivities and the Seebeck coefficient are about 2–5 %.

4. Conclusions

$(Bi_2Te_3)_{0.25}(Sb_2Te_3)_{0.75}$ as a TE element was fabricated. As the deficit of Te leads to the formation of unstoichiometric compound – $Sb_{0.405}Te_{0.595}$, the extra Te (at the amount of 0 to 4 wt%) was added to form $(Bi_2Te_3)_{0.25}(Sb_2Te_3)_{0.75}$ which is a chemically stoichiometric compound. The structure was tested by XRD, SEM, EBDS and AFM. More effective analysis methods such as AAS and Electron Probe Micro-Analyzer (EPMA) are strongly recommended to determine the exact chemical stoichiometry and impurities at ppm scale for efficiency improvement. The perfect nature of the crystal structure was confirmed by major improvement in the TE transport parameters that validate the structure modifications. TE parameters, electrical and thermal conductivities and the Seebeck coefficient measurements account for a higher quality of the crystals at 3 wt% addition of Te to the compounds. It is concluded that the purification processes of the TE elements in particular sulfur refinement have an important effect on the TE parameters.

References

[1] IOFFE A.F., *Semiconductor thermoelements and thermoelectric cooling*, Infosearch, London, 1957. P. 39.

[2] GOLDSMID H.J., *Electronic refrigeration*, Piton, London, 1986.

[3] HA H.P., CHO Y.W., BYUN J.Y., SHIM J.D., Proc. 12th Int. Conf. Thermoelectrics, Yokohama, Japan, 1993, p. 105.

[4] IVANOVA L.D., GRANATKINA YU.V., POLIKARPOVA N.V., SMIRNOVA E.I., *Inorg. Mater.*, 33 (1997), 558.

[5] ZAKERI M., ALLAHKARAMI M., KAVEI GH., KHANMOHAMMADIAN A., RAHIMIPOUR M.R., *J. Mater. Sci.*, 43 (2008),1638.

[6] ZAKERI M., ALLAHKARAMI M., KAVEI GH., KHANMOHAMMADIAN A., RAHIMIPOUR M.R., *J. Mater. Process. Tech.*, 209 (2009), 96.

[7] SEO J., PARK K., LEE D., LEE C., *Scr. Mater.*, 38 (1998), 477.

[8] HYUN D.B., HWANG J.S., SHIM J.D., OH T.S., *J. Mater. Sci.*, 36 (2001), 1285.

[9] TRITT T.M., *Science*, 283 (1999), 804.

[10] SMITH M.J., KNIGHT R.J., SPENCER C.W., *J. Appl. Phys.*, 33 (1962), 2186.

[11] OH T.S., HYUN B.D., KOLOMOEETS E.D., *Scripta Mater.*, 42 (2000), 849.

[12] KAVEI G., KARAMI M.A., *Bull. Mater. Sci.*, Vol. 29 № 7 (2006), 659.

[13] JIANG J., CHEN L., BAI S., YAO Q., WANG Q., *J. Cryst. Growth*, 277 (2005), 258.

[14] YANG J., AIZAWA T., YAMAMOTO A., OHTA T., *J. Alloy Comp.*, 309 (2000), 225.

[15] HEON P.H., YOUNG W.C., JI Y.B., JAE D.S., *J. Phys. Chem. Solids*, 55 (1994), 1233.

[16] KIM H.C., OH T.S., HYUN D.B., *J. Phys. Chem. Solids*, 61 (2000), 743.

[17] SMIROUS K., STOURAC L., *Z. Naturforsch. A*, 14 (1959), 848.

[18] ROSI F.D., HOCKINGS E.F., LINDENBLAD N.E., *RCA Rev.*, 22 (1961),82.

[19] XI'AN FAN, YANG J., ZHU W., BAO S., DUAN X., ZHANG Q., *J. Alloy Comp.*, Vol. 448 Issues 1–2 (2008), 308.

[20] SCHERRER H., HAMMOU B. AND SCHERRER S., *Phys, Lett. A*, 130 (1988), 161.

[21] HSU K.F., LOO S., GUO F., CHEN W., DYCK J.S., UHER C., HOGEN T., POLYCHRONIADIS E.K., KANATZIDIS M.G., *Science*, 303 (2004), 818.

[22] BIRDI K.S., *Scanning Prob Microscopes, Applications in Science and Technology*, CRC Press, Boca Raton, London, 2003.

[23] KAVEI G., ZARE Y., SEYYEDI A., *Journal of Thermoelectricity*, № 2 (2008), 57.

[24] A.V. PETROV, V.A. KUTASOV, *Thermoelectric properties of semiconductors (ed.) (New York: Consultants Bureau)*, (1964), p. 17.

[25] ALAM M.N., BLACKMAN M., PASHLEY D.W., High-angle Kikuchi Patterns, *Proc. Roy. Soc.*, 221 (1954), 224.

[26] BABA-KISHI K.Z., DINGLEY D.J., *J. Appl. Cryst.*, 22 (1989), 189.

[27] KAVEI G., KARAMI M.A., *Eur. Phys. J. Appl. Phys.*, 42 (2008), 67.

[28] UEMURA K., NISHIDA I., *Thermoelectric Semiconductors and their Applications*, Nikkan Kogyo Shinbun Press, Tokyo, 1988, p. 145.

[29] SEO J., PARK K., LEE D., LEE C., *Scripta Mater.*, 38 (1998), 477.

[30] IWAISOKO Y., AIZAWA T., YAMAMOTO A., OHTA T., *Jpn. J. Powder Metall.*, Vol. 45 № 10 (1998), 958.

Received 28.09.2010
Accepted 17.10.2011